Strategies and Considerations for Least-Squares Analysis of Total Scattering Data

Carolyne Chepkemboi,[†] Kyle Jorgensen,[†] Janell Sato,[†] and Geneva Laurita*

Read Online

ACCESS | 📊 Metrics & More | 📰 Article Recommendations

ABSTRACT: The process of least-squares analysis has been applied for decades in the field of crystallography. Here, we discuss the application of this process to total scattering data, primarily in the combination of least-squares Rietveld refinements and fitting of the atomic pair distribution function (PDF). While these two approaches use the same framework, the interpretation of results from least-squares fitting of PDF data should be done with caution through carefully constructed analysis approaches. We provide strategies and considerations for applying least-squares analysis to total scattering data, combining both crystallographic Rietveld and fitting of PDF data, given in context with recent examples from the literature. This perspective is aimed to be an accessible document for those new to the total scattering approach, as well as a reflective framework for the total scattering expert.
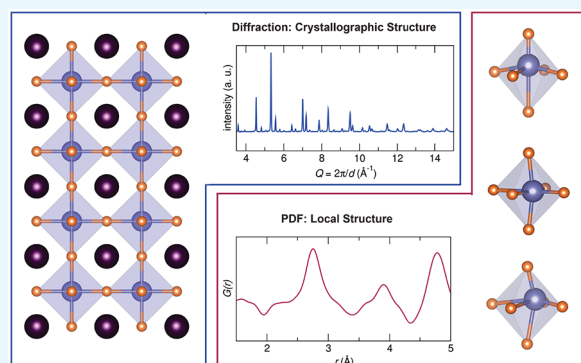
■ TOTAL SCATTERING AND CRYSTALLINE MATERIALS

The discovery of Bragg diffraction[1] in the early 1900s marked a breakthrough in the structural characterization of crystalline materials, allowing for a detailed description of the atomic arrangements that give rise to properties of interest. When a crystal is irradiated with a source that is approximately the distance between its atoms, the periodic array of atoms scatters the source to create an interference pattern. The constructively scattered waves result in a diffraction pattern which can be interpreted to yield valuable structural information. Diffraction has long been the standard for characterizing crystalline materials, and the analysis of these data has been advanced through the application of various mathematical methods such as whole pattern fitting and decomposition methods, including the Le Bail[2,3] and Rietveld[4] methods. Rigid and reliable, crystallography reigns supreme as the primary method for the characterization of highly crystalline materials.

With advances in high energy sources such as synchrotron X-ray and spallation neutron over the past few decades, new life has been given to the study of perfectly periodic materials in the form of the total scattering technique. This technique combines the analysis of both the Bragg scattering data from the diffraction experiment and diffuse scattering that is present in all materials, which can arise from structural defects or correlated motion between neighboring atoms. While much information can be gleaned about the global crystallographic structure from diffraction, numerous works over the past few decades have highlighted the importance of utilizing the pair distribution function (PDF) to study the local structure of

materials. Many crystallographically hidden structural features play an important role in explaining the properties of functional materials beyond what can be accessed via crystallographic techniques, and this understanding has allowed for advances in numerous technological areas.

In complex materials, it is crucial to garner an understanding of atomic behavior across multiple length scales. Crystallography describes the average structure of the material, but relies on the periodic nature of the material. If distortions in a material are correlated over long ranges in a repeating manner, such as cation off-centering in the same crystallographic direction, this will be captured in the average structure (illustrated in Figure 1a). However, if the local environment is distorted but in an incoherent, uncorrelated manner (for example, cation off-centering in different directions from one cation environment to the next), it will result in an average of the positions, and in the crystallographic structure, the cation appears to be located in the center of the coordination environment with an enlarged atomic displacement parameter (ADP, illustrated in Figure 1b). Therefore, the structure determined from diffraction is a less precise and potentially inaccurate representation of the symmetry around the cation,
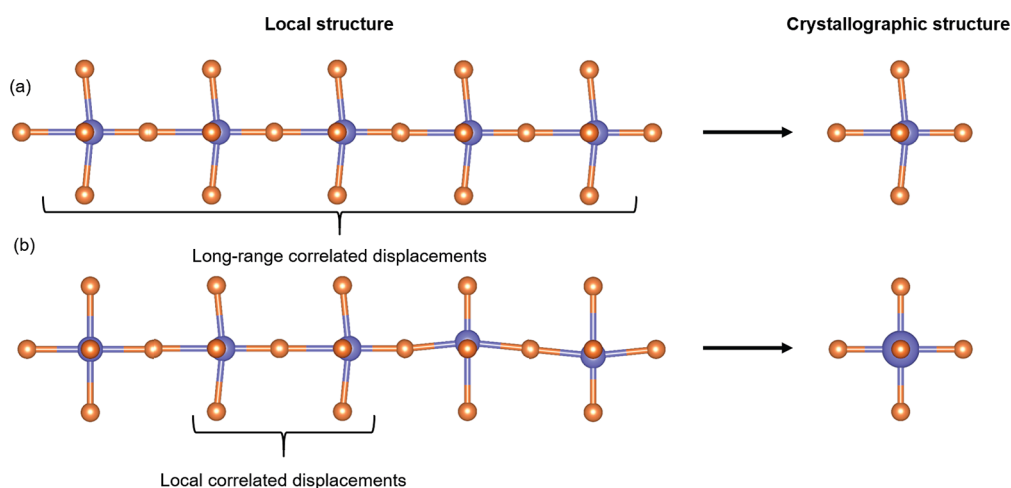
**Figure 1.** Illustration of local and average structures of two materials: (a) correlated off-centering displacements in the local structure are observed as a crystallographically off-centered structure; (b) local off-centering that is either not correlated or only correlated to a nearest neighbor (local correlated displacements) manifest in the crystallographic structure with an enlarged atomic displacement parameter that is not representative of the local coordination environment.
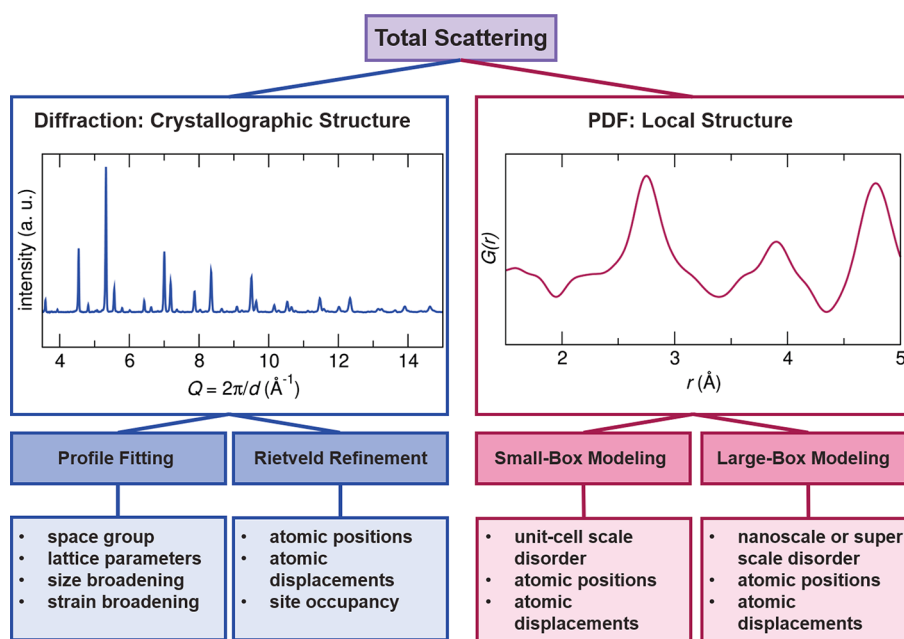
Figure 2. Common data analysis strategies for total scattering data. Structural data can be extracted from the reciprocal space diffraction data (left) through methods such as profile fitting and Rietveld refinement and from the real-space PDF data (right) through methods such a small- and large-box modeling.

which leads to inaccurate conclusions about the bonding and orbital overlap of the atoms in the material. These limits of average structure methods can be overcome using PDF to understand the local bonding and atomic arrangement of the structure.

The PDF is a histogram of all atom−atom interactions in a material and does not necessarily rely on Bragg diffraction; PDF analysis can be applied to any type of material with careful consideration. Originally applied to glasses and amorphous materials,[5−7] PDF analysis is finding strength in characterizing a wide array of materials based on analysis over various length scales: from characterization of molecular compounds,[8] to analysis of the coordination environments in noncrystalline and nanostructured materials,[9,10] to describing the structural interactions in a single nanoparticle,[11,12] to

characterizing the mid- and long-range atomic interactions in semi- and highly crystalline materials.[13−15] Many works have been produced to summarize and illustrate the advantages of this technique across a variety of materials, and is it highly recommended to consult these works to understand the methodology[16−19] and variety of applications.[13−15,20−22]

This contribution focuses on recent successes in applying the total scattering method to highly crystalline materials, where both Bragg and diffuse scattering is analyzed using a least-squares modeling approach. In particular, we highlight a few key strategies for total scattering analysis when considering materials that have been extensively characterized through crystallographic techniques. This perspective aims to illustrate the strengths of this technique while providing important considerations for its application, particularly in the distinction

between crystallographic and local structure analysis. The theme of this work is that there is no "one size fits all" approach to analyzing total scattering data, and valuable information can be extracted from a variety of strategies beyond a perfect fit to the structural data.

■ LEAST-SQUARES ANALYSIS AND TOTAL SCATTERING DATA

The analysis of total scattering data is typically performed by modeling the diffraction and PDF data against an initial structural model, which is then modified to improve the difference between the experimental data and the calculated scattering data from the model. The average structure is typically modeled against a complete diffraction pattern (whole pattern fitting methods) with a number of diffraction planes collected over a range of diffraction angles. The local structure can be subsequently or independently analyzed through small- or large-box modeling approaches. A framework for common analysis strategies of total scattering data is presented in Figure 2. Both whole pattern fitting and small-box modeling utilize least-squares methods to fit the data against a known structural model and is the focus of this contribution.

The least-squares refinement is an iterative multistep process that aims to minimize the difference between the observed and calculated data. In each step, or cycle, of the refinement, the model improves and is used as the starting point for the next cycle. The accuracy of the model can be assessed through various "goodness-of-fit" metrics, and a thorough comparison of the metrics based on diffraction analysis can be found elsewhere.[23] The most commonly used are χ^2 and R_w, and in both cases, the smaller the number, the smaller the difference between observed and calculated patterns and the more accurately the structural model describes the data. In a least-squares approach, the process will converge on the difference (or minimum) that is achievable based on small variations in the refinable parameters. Therefore, the starting model must be close to the final model, or the global minimum may not be achieved.

Whole pattern fitting includes pattern decomposition methods, such as the Pawley[24] and LeBail[3] methods, and the Rietveld method,[4] which is the primary focus of this contribution. For the calculated pattern, reflections are generated based on the space group and unit cell parameters of the structural model. The generation of peak intensity at each position is specific to the selected method. In a Rietveld refinement, intensities are generated based on the scattering power of atoms in the diffraction plane of that reflection. The peak positions and intensities of the calculated pattern are adjusted through the refinement of the lattice parameter, atomic positions, displacement parameters, and site occupancies. In addition to refined structural parameters, the profile of the peak and background shape can be modeled through the refinement of instrumental parameters and incorporation of intensity corrections such as sample or atom-specific absorption. In this case, any scattering that is not due to Bragg events is treated as an additional factor in the algorithm of the model, only extracting structural data from the Bragg peaks. While this is satisfactory for crystallographic analysis, many of the diffuse scattering events that arise from local distortions manifest in the background of the data and are thus lost through this modeling approach.

The concept of applying a full-profile fitting regression technique to the atomic pair distribution function was led by

Simon Billinge and collaborators in the RESPAR, or "Real Space Rietveld", program.[25] Similar to a Rietveld refinement, this method assumes that a structure can be described by a small number of atoms in a unit cell or small super cell, hence the descriptor small-box modeling that often accompanies this technique. Similar variables can be refined against this small atomic model, allowing for the extraction of structural details such as the atomic coordinates, displacement parameters, and site occupancies. This program provided the foundation for the PDFfit[26] and PDFfit2[27] programs, the latter of which is implemented in the open source graphical user interface PDFgui.[27] With this approach, the refined variables or parameters are intentionally in direct analogy to those in crystallography; however, as with any analysis of powder diffraction data, the structural solutions are not unique and care must be taken in the interpretation of modeling results. For example, there are many contributing factors to the peak width in the PDF, such as disorder of atoms on their atomic sites, correlated motion of neighboring atoms (which results in sharper peaks at low r and broader peaks at high r), or overlapping peaks at a given radial distance. Therefore, is it important to be cognizant of the factors that are arising from the chemistry of the sample (such as static atomic displacements causing multiple bond lengths, dynamic displacements inducing additional disorder, or an impurity phase) versus parameters that are mostly used to improve the description of the peak shape (correlated motion functions). As with any refinement, it is crucial to be transparent about any refined parameters when reporting the analysis of PDF data. Additionally, unlike a diffraction pattern, where the entire range of data is fit, the real-space r range that the data are fit against must be specified by the user. This flexibility allows the user to understand structural characteristics on various length scales but also challenges the user to consider the appropriateness of the length scale for the derivation of structural features. For example, if PDF data are being utilized to determine the lattice parameter of a material, the fit range should at the very least cover the entire length scale of a unit cell.

A criteria of the least-squares approach is that the starting model must be close to the final model, as the iterations of the refinement involve small changes in the variable parameters. In a case where the local structure is vastly different from the average structure and candidate models for the distortions are not known, a large-box approach such as reverse Monte Carlo (RMC) modeling is often more appropriate.[28] RMC modeling yields a much larger number of nonunique structural solutions than small-box modeling. Given this outcome, it is highly advisable to perform an RMC simulation against multiple data sets, including the Bragg diffraction (if available) and PDF data. Improvements in minimizing the number of unique solutions can be achieved through the use of chemical constraints such as fixed coordination numbers or bond valence sums on a given atom. There are a number of examples on how to apply this approach to materials,[29−32] but that is beyond the focus of this current paper.

Solving a structure from diffraction data, particularly single crystal data, is a common technique, and powder diffraction and Rietveld analysis can yield robust results pertaining to the accuracy of the crystallographic model. A common pitfall for new practitioners to the total scattering approach is that the local structure should be "solved" in a manner similar to that of a single crystal or whole pattern powder experiment. While

similar metrics can be obtained from fitting PDF data, the resulting structural model should be carefully scrutinized for chemical consistency (for example, reasonable bond lengths or positive atomic displacement parameters). This is particularly important when modeling the data over a very short length scale, as the number of peaks fit against the model is limited. As with any type of analysis against a structural model, it is important to check that the goal is not simply to achieve the lowest χ^2 or R_w value. The final check should be to look critically at the analysis to monitor for any obvious regions of mismatch between the data and the fit.

Given the additional steps of data reduction, the varying contributions to the peaks in a PDF, and the various real-space length scales over which the PDF can be analyzed, a well-constructed comparative analysis is the most effective approach for understanding the local structure of a material. In the following section, we expand on some useful strategies and literature examples that highlight extracting structural information from crystalline materials with underlying local distortions.

## ◼ STRATEGIES FOR LEAST-SQUARES ANALYSIS OF TOTAL SCATTERING DATA

Total scattering is an ideal tool for probing crystalline materials that have local distortions that do not correlate over long ranges. These local distortions may be hinted at in the crystallographic analysis but cannot be accurately captured by a crystallographic modeling approach. For example, large contributions to the background noise or enlarged atomic displacement parameters may suggest underlying disorder that cannot be incorporated into a periodic crystalline model. When utilizing total scattering to describe structural characteristics across a range of length scales in a crystalline material, there are several approaches for modeling the data beyond an absolute solution to the local structure. While not exhaustive, in the following section, we illustrate a few comparative strategies in the context of recent literature examples to understand distortions across various length scales.

Qualitative Deviations from the Crystalline Model. A natural way to think about modeling the local structure is to use a framework similar to a crystallographic Rietveld analysis. Small-box modeling can be used to describe the local structure over various r ranges through the refinement of variables similar to those in a Rietveld refinement using a crystalline model. While similar in process, it is important to note that when modeling PDF data against a crystallographic structure, you are only describing the structure over the length scale indicated in the fitting parameters. This can be performed using programs such as PDFgui,[27] and while a structural model is used that contains a space group, space groups rely on translational symmetry, and this may or may not be a valid assumption given the length scale over which the data are being fit. Even so, the arrangement of atoms, with or without translational symmetry, will give rise to a pairwise interaction pattern, and this can be compared to the data to elucidate the arrangement of atoms from a local to global scale.

An excellent place to start is to simply fit the local structure against the crystallographic structure obtained through Rietveld analysis. In some cases, the local structure is well-described by the crystalline model,[34−37] and it can be concluded that the local and average structure are the same. However, this is not the case in a variety of materials.[33,38−53] In these cases, areas of the PDF that are not well-described by the

crystallographic structure can provide insight into the nature of a local distortion, for example an M−O peak (i.e., a bond length) that shows a large discrepancy between the data and the fit.

This idea is illustrated in Figure 3, which highlights recent work by Shi et al.[33] Working to understand metastable phase
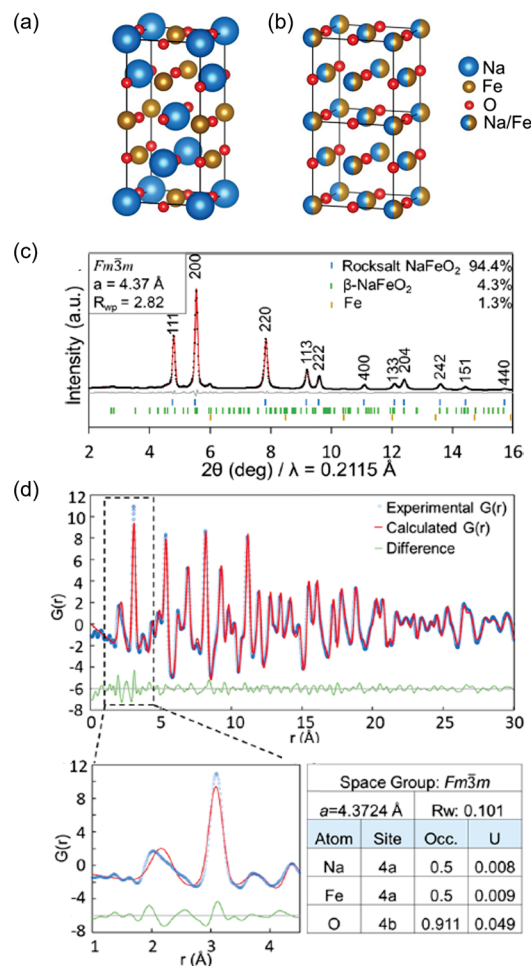
Figure 3. Total scattering (X-ray, 11-ID-B, APS) of NaFeO$_2$ synthesized via a martensitic-like phase transformation from β-NaFeO$_2$ (a). The data were fit against an disordered rocksalt crystal model (b), which is a good description of the diffraction data (c). This crystallographic model was used to fit the PDF data (d), and while the data are fit well at high r values, the inset highlights that this is not a good structural model for the local peaks below 4 Å, attributed to high disorder indicated by an elevated U_{iso} on the O site. Figure adapted from ref 33. Copyright 2018 American Chemical Society.

synthesis, the team used a mechanochemical method to prepare a new metastable phase of NaFeO$_2$ from the high-temperature β-NaFeO$_2$ phase of the composition (Figure 3a). It can be seen in Figure 3c that a disordered rocksalt structure (Figure 3b) is a good model of the crystallographic data, indicated by the relatively flat difference curve and a low R_{wp}. When applied to the PDF data, shown in Figure 3d, the data are well-described at longer length scales. However, when focusing on the local coordination environments of the cations from 1 to 4.5 Å, it can be observed that the structural model does not appropriately describe the local bond lengths. This disorder is further evidenced by an elevated U_{iso} on the oxygen
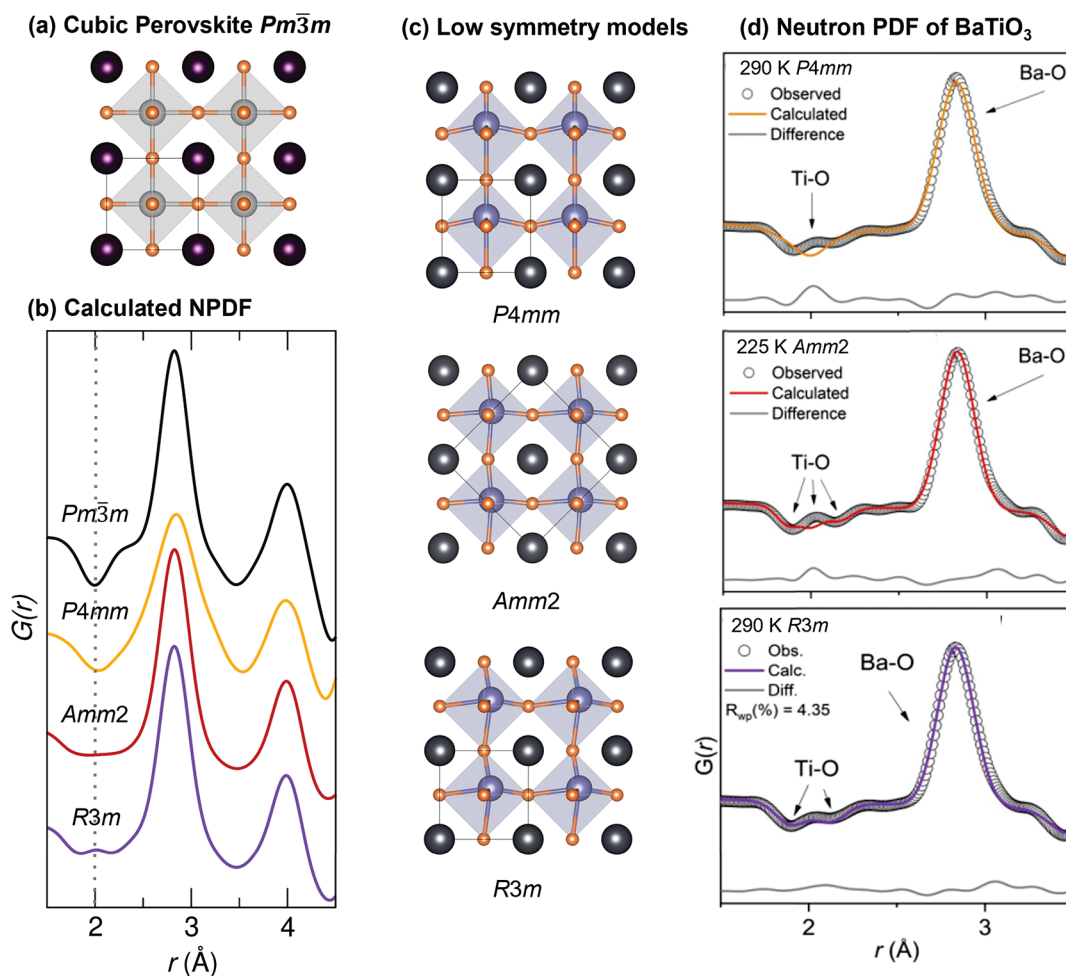
Figure 4. (a) High-temperature cubic pervoskite structure. (b) Calculated neutron PDFs from (c) prototypical ferroelectric phases with exaggerated Ti displacements shown for clarity. (d) Fits to PDF data (neutron, NOMAD, SNS) of BaTiO$_3$ at 290 K (top and bottom panels) and 225 K (middle panel). Figure adapted in part with permission from ref 54. Copyright 2020 Springer Nature.

site, indicating that the oxygen positions are not accurately described by the disordered rocksalt model. Combined with a suite of other local and bulk characterization tools, PDF helped provide crucial information toward controlled synthesis of this new metastable phase. While not quantitative in terms of the local arrangement of atoms, this qualitative approach can provide meaningful insight into deviations from the crystallographic structure that may have consequential implications on the formation of a phase or on the observed properties of interest.

Quantitative Modeling with Low-Symmetry Subgroups. When the crystallographic model does not describe the local structure, comparative analysis with lower-symmetry space groups than that of the average structure can provide a more quantitative answer. When modeling PDF data, structural candidates can be chosen using symmetry group−subgroup relationships or based on the various structural features expected at a given length scale. For example, in the case of a distorted coordination environment (such as cation off-centering), fitting the data up to approximately 6 Å should capture any M−X or intraoctahedral X−X interactions (where M is a cation and X is an anion). However, if the question is on a longer scale, such as octahedral tilting, it would be better to fit the data over a length scale that would capture interoctahedral M−M and X−X interactions.

Many examples of this approach can be found in the literature,[55−68] particularly in describing local distortions in perovskite materials. Perovskites have the advantage of being thoroughly characterized through crystallographic[69−75] and computational[76,77] methods, and the various lower-symmetry distortions and phase transitions are well-classified, providing a library of structures to fit data against. A classic example is that of BaTiO$_3$, which has the cubic $Pm\bar{3}m$ structure at high temperatures (Figure 4a visualized using VESTA[78]). Crystallographically, both the Ba and Ti are centered in their coordination environments, and upon cooling, the second-order Jahn−Teller active Ti^{4+} off-centers toward the corner of the octahedra in the $P4mm$ structure, then toward the edge of the octahedra in the $Amm2$ structure, and finally toward the face of the octahedra in the $R3m$ structure (Figure 4c).[69,70] These three phases give distinct signatures in the PDF data, particularly when neutron scattering is used as a probe due to the considerable contrast afforded from the negative scattering cross section of Ti (shown in Figure 4b as calculated PDFs generated in PDFgui[27]). Local analysis[11,79,80] against these candidate space groups indicates that the $R3m$-type distortion persists at much higher temperatures but is incoherent and thus averages out to the observed crystallographic phases, resulting in an order−disorder series of phase transitions.[80−83] Recent investigations on the local structure of BaTiO$_3$ through
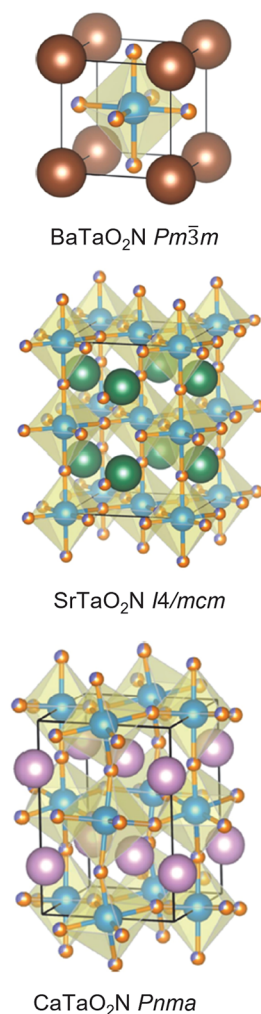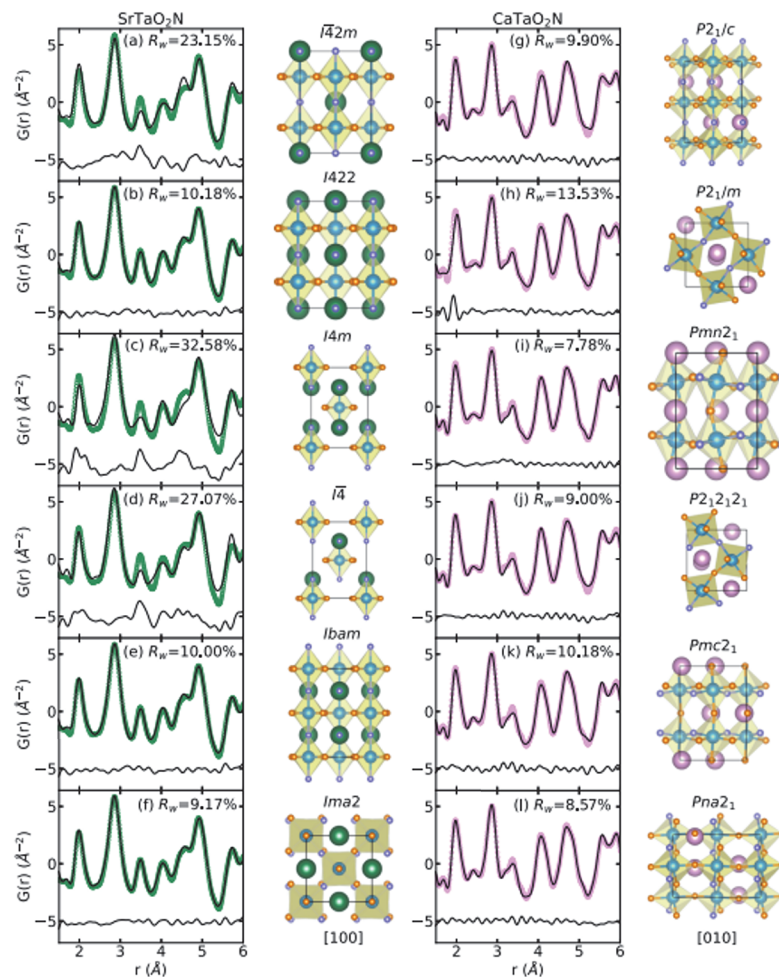
Figure 5. (a) Refined crystallographic structures for mixed-anion perovskites $MTaO_2N$ (M = Ba, Sr, and Ca). (b) Fits of the room temperature data (neutron, NPDF, LANSCE) against low-symmetry models with various anion ordering and octahedral tilting for compositions $SrTaO_2N$ and $CaTaO_2N$. Figure adapted from ref 71. Copyright 2021 American Chemical Society.

the orthorhombic $Amm2$ to tetragonal $P4mm$ global phase transition (Figure 4d) confirm the rhombohedral $R3m$ persists locally through this region and detailed the coherence length of the rhombohedral-type displacements of Ti at these temperatures.[54] This local behavior has a major impact on the properties of $BaTiO_3$: the long-range correlation of local dipoles allows for large permittivities[84,85] and ferroelectric behavior,[86] making it a valuable material for a number of technological applications. Understanding the origin of these properties and how to manipulate and induce similar structural distortions in other materials is a key factor in driving technological innovations.

Similar types of local distortions ($R3m$-, $Amm2$-, or $P4mm$-type) can be observed across a variety of perovskite chemistries, such as in a variety of other perovskite oxides[48,87] and halide perosvkites.[72,75,88,89] By applying well-established perosvkite metrics such as the Goldschmidt tolerence factor[90] and Glazer "tilt systems",[91] a comprehensive comparison of suspected low-symmetry space groups can be applied to any perovskite system beyond those of the prototypical ferroelectric subgroups. This approach has also been recently applied to mixed anion perovskites $MTaO_2N$,[71] where an

extensive number of low-symmetry perovskite structures were fit against the data to garner the most accurate description of the local structure (Figure 5). In combination with density functional theory and ab initio molecular dynamics simulations, modeling of the total scattering data provided a framework for predicting anion ordering, which has a direct consequence on the stability of various mixed-anion perovskite phases.

Detailed here for the perovskites due to the vast supporting literature, the framework of utilizing group−subgroup relationships and known low-temperature phase transitions can be applied to any structure type. When performing fits against lower-symmetry space groups, it should be noted that a better fit (i.e., a lower χ^2 or R_w value) might be achieved simply by increasing the number of refined variables. Therefore, it is important to constrain, or not to refine, any variables that are confidently known (such a a correlated motion parameter or a site occupancy) to minimize the number of variables. Several factors can additionally be checked to support the validity of a low-symmetry space group, such as smaller U_{iso} values than the high-symmetry model, reasonable error associated with refined parameters, and a lack of correlation between refined
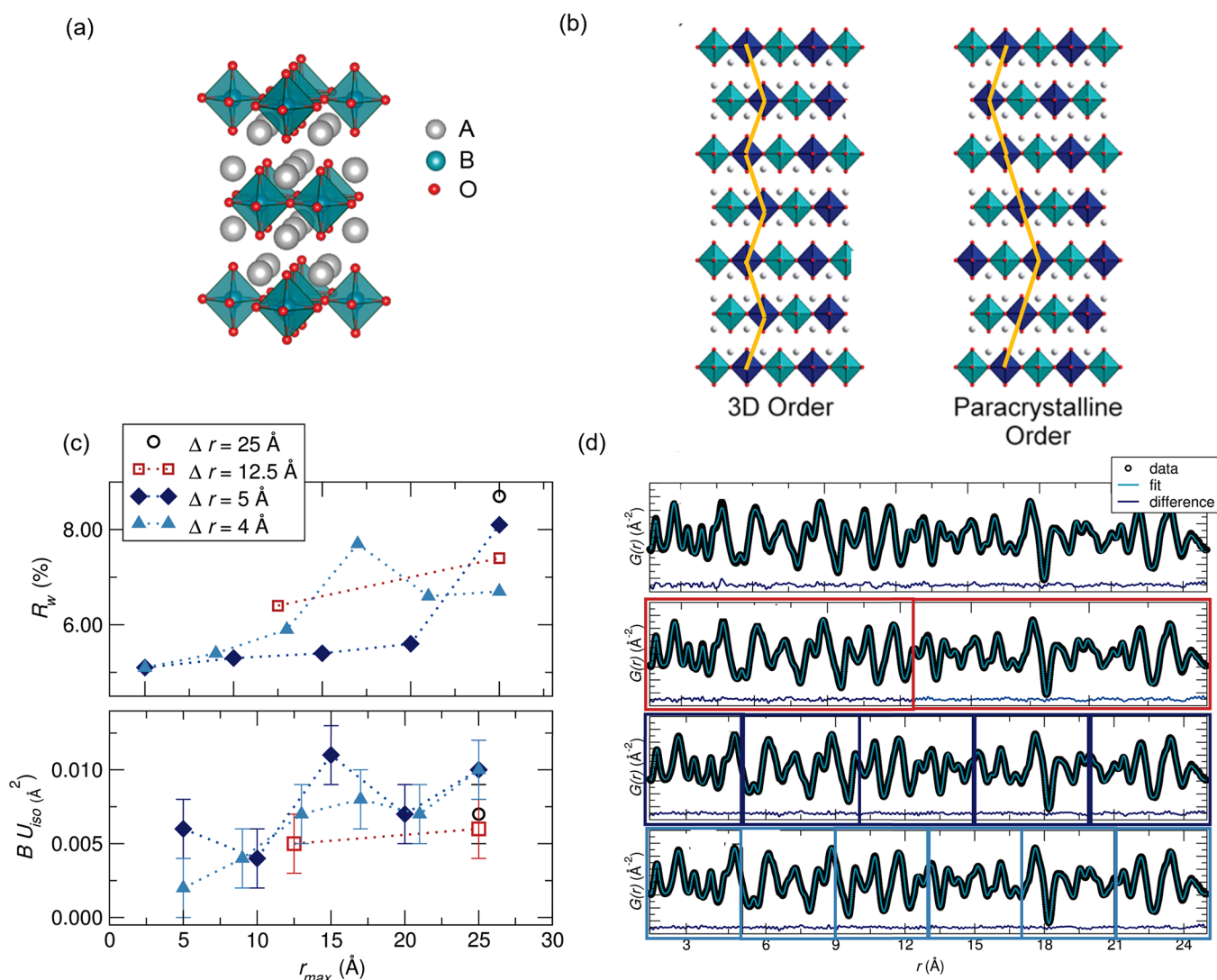
Figure 6. (a) A_2BO_4, $n = 1$ Ruddlesden−Popper structure (b) shown with the arrangement of B-cations (dark and light blue) in 3D-ordered and 2D paracrystalline ordered phases with the registry between dark blue cations highlighted with a yellow line. (c) R_w and U_{iso} values obtained from fitting the neutron PDF data over various r range box-cars (Δr) as a function of r_{max}, the upper bound of each box-car in the series. An apparent worsening of the fit (indicated by an elevated R_w and B-site U_{iso}) is observed over the next nearest neighbor region of the PDF (approximately 12−13.5 Å), indicating paracrystalline order. (d) Fits of the PDF data (neutron, NOMAD, SNS) against a 3D-ordered model across various highlighted r range box-cars (Δr) corresponding to the legend colors in (c). Figure adapted from ref 98. Copyright 2020 American Chemical Society.

parameters. Once a more quantitative model of the local structure has been obtained a more detailed analysis of the bonding and orbital overlap can be considered, which is of paramount importance to fully understanding phase formation or observed properties.

Length-Scale-Dependent Box-Car Analysis. Discrete modeling of local coordination environments can provide answers beyond crystallography, but many times a material's functionality is a combination of interactions across different length scales. A targeted approach to understanding multiscale interactions at play in a material is the box-car method.[60,73,92−97] In this method, fits are performed by taking a set increment of r range, for example, 5 Å, and fitting the data against a candidate model at various length scales with this increment (i.e., 0−5, 5−10, 10−15 Å, etc.). A comparison of the derived parameters from each box-car, such as the R_w or U_{iso}, can indicate the interaction lengths where the model deviates from the data. This finds particular strength in independently describing any midrange features (between

approximately 5 and 20 Å) that may not be obvious over a local or long-range fit.

A recent example of the influence of midrange interactions is in the suspected paracrystalline Ruddlesden−Popper phase of $LaSr_3NiRuO_8$ (Figure 6).[98] This layered material is described as intergrown layers of rocksalt and perovskite-type atomic arrangements, and as with many layered materials, the registry between layers is prone to disorder. In addition to layer-induced disorder, the perovskite-type layer in $LaSr_3NiRuO_8$ contains an equal mix of Ni^{2+} and Ru^{5+} cations, and the atomic arrangement (disordered versus ordered on the crystallographic site) influences the magnetic response of the material. It was determined through crystallographic techniques that the Ni^{2+} and Ru^{5+} cations were disordered. This was directly contrasted by the observed antiferromagnetic magnetic behavior of the material, which would arise from cation order in the material. To investigate this discrepancy, PDF was employed to characterize the material across a variety of length scales. The sample was fit against a cation-ordered model

across various box-cars (Figure 6d), and it was discovered that the model had the worst fit to the data between 12 and 15 Å (Figure 6c), which corresponds to the intralayer spacing in the material. This evidenced a paracrystalline structure of the material: cations were ordered within the plane of a given layer, but the layers do not stack perfectly on top of each other. This explains both the observed magnetic ordering and disordered crystallographic structure and illustrates the necessity to study materials beyond the local and crystallographic scale.

■ CONCLUSIONS AND BEST PRACTICES

With increasing capabilities and upgrades to synchrotron and spallation sources across the world, total scattering is becoming a leading technique for understanding the structural behavior of crystalline materials across a range of length scales. Through the combination of Rietveld and PDF, a holistic understanding of the structural origins of functionality is possible. In particular, the process of least-squares analysis can be applied in creative and comparative ways, and one does not have to find the perfect fit to make meaningful connections between structure and properties. We have illustrated examples for qualitative and quantitative analysis, including box-car analysis of multilength scale studies. For the new practitioner, there is an abundance of literature on useful ways to study a material through total scattering techniques, and this contribution has merely scratched the surface of what can be done. With this in mind, it is important to remember that least-squares analysis is not a black-box technique, and a careful construction of the analysis and chemical factors at play should always be incorporated. If feasible, the incorporation of other local probes such as NMR, XAS, IR, or Raman spectroscopy can aid in the interpretation. In combination, total scattering is a powerful technique that can elucidate a variety of structural interactions, enabling the understanding of structure−property relationships that can be tuned or promoted in materials.

■ AUTHOR INFORMATION

Corresponding Author

Geneva Laurita − *Department of Chemistry and Biochemistry, Bates College, Lewiston, Maine 04240-6020, United States;* ⊙ orcid.org/0000-0001-9577-150X; Email: glaurita@bates.edu

Authors

Carolyne Chepkemboi − *Department of Chemistry and Biochemistry, Bates College, Lewiston, Maine 04240-6020, United States*

Kyle Jorgensen − *Department of Chemistry and Biochemistry, Bates College, Lewiston, Maine 04240-6020, United States*

Janell Sato − *Department of Chemistry and Biochemistry, Bates College, Lewiston, Maine 04240-6020, United States*

Complete contact information is available at:
https://pubs.acs.org/10.1021/acsomega.2c01285

Author Contributions

†C.C., K.J., and J.S. contributed equally to this work.

Notes

The authors declare no competing financial interest.

■ ACKNOWLEDGMENTS

■ REFERENCES

(1) Bragg, W. H.; Bragg, W. L. The reflection of X-rays by crystals. *Proc. R. Soc. London A* **1913**, *88*, 428−438.

(2) Le Bail, A.; Duroy, H.; Fourquet, J. Ab-initio structure determination of $LiSbWO_6$ by X-ray Powder Diffr. *Mater. Res. Bull.* **1988**, *23*, 447−452.

(3) Le Bail, A. Whole Powder Pattern Decomposition Methods and Applications: A Retrospection. *Powder Diffr* **2005**, *20*, 316−326.

(4) Rietveld, H. M. A Profile Refinement Method for Nuclear and Magnetic Structures. *J. Appl. Crystallogr.* **1969**, *2*, 65−71.

(5) Debye, P.; Menke, H. The determination of the inner structure of liquids by X-ray means. *Phys. Z.* **1930**, *31*, 797−798.

(6) Tarasov, L. P.; Warren, B. E. X-Ray Diffraction Study of Liquid Sodium. *J. Chem. Phys.* **1936**, *4*, 236−238.

(7) Warren, B. E.; Krutter, H. M.; Morningstar, O. Fourier Analysis of X-ray Patterns of Vitreous SiO_2 and B_2O_3. *J. Am. Ceram. Soc.* **1992**, *75*, 11−15.

(8) Terban, M. W.; Billinge, S. J. L. Structural Analysis of Molecular Materials Using the Pair Distribution Function. *Chem. Rev.* **2022**, *122*, 1208−1272.

(9) Billinge, S. J. L.; Kanatzidis, M. G. Beyond crystallography: the study of disorder, nanocrystallinity and crystallographically challenged materials with pair distribution functions. *Chem. Commun.* **2004**, 749−760.

(10) Billinge, S. J. L.; Levin, I. The Problem with Determining Atomic Structure at the Nanoscale. *Science* **2007**, *316*, 561−565.

(11) Page, K.; Proffen, T.; Niederberger, M.; Seshadri, R. Probing Local Dipoles and Ligand Structure in $BaTiO_3$ Nanoparticles. *Chem. Mater.* **2010**, *22*, 4386−4391.

(12) Luo, S.; Li, M.; Fung, V.; Sumpter, B. G.; Liu, J.; Wu, Z.; Page, K. New Insights into the Bulk and Surface Defect Structures of Ceria Nanocrystals from Neutron Scattering Study. *Chem. Mater.* **2021**, *33*, 3959−3970.

(13) Toby, B. H.; Egami, T. Accuracy of pair distribution function analysis applied to crystalline and non-crystalline materials. *Acta Crystallogr. A* **1992**, *48*, 336−346.

(14) Dove, M. T.; Tucker, M. G.; Keen, D. A. Neutron total scattering method: simultaneous determination of long-range and short-range order in disordered materials. *Eur. J. Mineral* **2002**, *14*, 331−348.

(15) Keen, D. A.; Goodwin, A. L. The crystallography of correlated disorder. *Nature* **2015**, *521*, 303−309.

(16) Keen, D. A. A comparison of various commonly used correlation functions for describing total scattering. *J. Appl. Crystallogr.* **2001**, *34*, 172−177.

(17) Proffen, T.; Billinge, S. J. L.; Egami, T.; Louca, D. Structural analysis of complex materials using the atomic pair distribution function — a practical guide. *Zeitschrift für Kristallographie - Crystalline Materials* **2003**, *218*, 132−143.

(18) Olds, D.; Saunders, C. N.; Peters, M.; Proffen, T.; Neuefeind, J.; Page, K. Precise implications for real-space pair distribution function modeling of effects intrinsic to modern time-of-flight neutron diffractometers. *Acta Crystallogr. A* **2018**, *74*, 293−307.

(19) Peterson, P. F.; Olds, D.; McDonnell, M. T.; Page, K. Illustrated formalisms for total scattering data: a guide for new practitioners. *J. Appl. Crystallogr.* **2021**, *54*, 317−332.

(20) Egami, T. *Underneath the Bragg Peaks Structural Analysis of Complex Materials*, 2nd ed.; Pergamon materials series; Pergamon: Amsterdam, 2012; Vol. *16*.

(21) Mancini, A.; Malavasi, L. Recent advances in the application of total scattering methods to functional materials. *Chem. Commun.* **2015**, *51*, 16592−16604.

(22) O'Quinn, E. C.; Sickafus, K. E.; Ewing, R. C.; Baldinozzi, G.; Neuefeind, J. C.; Tucker, M. G.; Fuentes, A. F.; Drey, D.; Lang, M. K.

Predicting short-range order and correlated phenomena in disordered crystalline materials. *Sci. Adv.* **2020**, *6*, No. eabc2758.

(23) Toby, B. H. R. factors in Rietveld analysis: How good is good enough? *Powder Diffr* **2006**, *21*, 67−70.

(24) Pawley, G. S. Unit-cell refinement from Powder Diffr. scans. *J. Appl. Crystallogr.* **1981**, *14*, 357−361.

(25) Billinge, S. J. L. In *Local Structure from Diffraction*; Billinge, S. J. L., Thorpe, M. F., Eds.; Springer: Boston, MA, 2002; pp 137−156.

(26) Proffen, T.; Billinge, S. J. L. *PDFFIT*, a program for full profile structural refinement of the atomic pair distribution function. *J. Appl. Crystallogr.* **1999**, *32*, 572−575.

(27) Farrow, C. L.; Juhas, P.; Liu, J. W.; Bryndin, D.; Božin, E. S.; Bloch, J.; Proffen, T.; Billinge, S. J. L. PDFfit2 and PDFgui: computer programs for studying nanostructure in crystals. *J. Phys.: Condens. Matter* **2007**, *19*, 335219.

(28) McGreevy, R. L.; Pusztai, L. Reverse Monte Carlo Simulation: A New Technique for the Determination of Disordered Structures. *Mol. Simul* **1988**, *1*, 359−367.

(29) Keen, D. A.; Tucker, M. G.; Dove, M. T. Reverse Monte Carlo modelling of crystalline disorder. *J. Condens. Matter Phys.* **2005**, *17*, S15−S22.

(30) Aoun, B. Fullrmc, a rigid body reverse monte carlo modeling package enabled with machine learning and artificial intelligence. *J. Comput. Chem.* **2016**, *37*, 1102−1111.

(31) Tucker, M. G.; Keen, D. A.; Dove, M. T.; Goodwin, A. L.; Hui, Q. RMCProfile: reverse Monte Carlo for polycrystalline materials. *J. Condens. Matter Phys.* **2007**, *19*, 335218.

(32) Evrard, G.; Pusztai, L. Reverse Monte Carlo modelling of the structure of disordered materials with RMC: a new implementation of the algorithm in C. *J. Condens. Matter Phys.* **2005**, *17*, S1−S13.

(33) Shi, T.; Xiao, P.; Kwon, D.-H.; Sai Gautam, G.; Chakarawet, K.; Kim, H.; Bo, S.-H.; Ceder, G. Shear-Assisted Formation of Cation-Disordered Rocksalt $NaMO_2$ (M = Fe or Mn). *Chem. Mater.* **2018**, *30*, 8811−8821.

(34) Xu, Y.; Feygenson, M.; Page, K.; Nickles, L. S.; Brinkman, K. S. Structural Evolution in Hollandite Solid Solutions Across the A-Site Compositional Range from $Ba1.33Ga2.66Ti5.34O16$ to $Cs1.33Ga1.33Ti6.67O16$. *J. Am. Ceram. Soc.* **2016**, *99*, 4100−4106.

(35) Wang, J.; Lebedev, O. I.; Lee, K.; Dolyniuk, J.-A.; Klavins, P.; Bux, S.; Kovnir, K. High-efficiency thermoelectric $Ba_8Cu_{14}Ge_6P_{26}$: bridging the gap between tetrel-based and tetrel-free clathrates. *Chem. Sci.* **2017**, *8*, 8030−8038.

(36) Porter, Z.; Zoghlin, E.; Britner, S.; Husremovic, S.; Ruff, J. P. C.; Choi, Y.; Haskel, D.; Laurita, G.; Wilson, S. D. Evolution of structure and magnetism across the metal-insulator transition in the pyrochlore iridate $(Nd_{1−x}Ca_x)_2 Ir_2O_7$. *Phys. Rev. B* **2019**, *100*, 054409.

(37) Hermus, M.; Mansouri Tehrani, A.; Brgoch, J. Determining a Structural Distortion and Anion Ordering in La2Si4N6C via Computation and Experiment. *Inorg. Chem.* **2016**, *55*, 9454−9460.

(38) Palomares, R. I.; Tracy, C. L.; Neuefeind, J.; Ewing, R. C.; Trautmann, C.; Lang, M. Thermal defect annealing of swift heavy ion irradiated ThO2. *Nuclear Instruments and Methods in Physics Research Section B: Beam Interactions with Materials and Atoms* **2017**, *405*, 15−21.

(39) Drey, D. L.; O'Quinn, E. C.; Subramani, T.; Lilova, K.; Baldinozzi, G.; Gussev, I. M.; Fuentes, A. F.; Neuefeind, J. C.; Everett, M.; Sprouster, D.; Navrotsky, A.; Ewing, R. C.; Lang, M. Disorder in $Ho_2Ti_{2x}Zr_xO_7$: pyrochlore to defect fluorite solid solution series. *RSC Adv.* **2020**, *10*, 34632−34650.

(40) Zoghlin, E.; Schmehr, J.; Holgate, C.; Dally, R.; Liu, Y.; Laurita, G.; Wilson, S. D. Evaluating the effects of structural disorder on the magnetic properties of $Nd_2Zr_2O_7$. *Phys. Rev. Materials* **2021**, *5*, 084403.

(41) Thygesen, P. M. M.; Paddison, J. A. M.; Zhang, R.; Beyer, K. A.; Chapman, K. W.; Playford, H. Y.; Tucker, M. G.; Keen, D. A.; Hayward, M. A.; Goodwin, A. L. Orbital Dimer Model for the Spin-Glass State in $Y_2Mo_2O_7$. *Phys. Rev. Lett.* **2017**, *118*, 067201.

(42) Shanbogh, P. P.; Raghunathan, R.; Swain, D.; Feygenson, M.; Neuefeind, J.; Plaisier, J.; Narayana, C.; Rao, A.; Sundaram, N. G.

Impact of Average, Local, and Electronic Structure on Visible Light Photocatalysis in Novel $BiREWO_6$ (RE = Eu and Tb) Nanomaterials. *ACS Appl. Mater. Interfaces* **2018**, *10*, 35876−35887.

(43) Ma, Y.; Wang, Q.; Li, C.; Santodonato, L. J.; Feygenson, M.; Dong, C.; Liaw, P. K. Chemical short-range orders and the induced structural transition in high-entropy alloys. *Scr. Mater.* **2018**, *144*, 64−68.

(44) Lin, K.; et al. Strong Second Harmonic Generation in a Tungsten Bronze Oxide by Enhancing Local Structural Distortion. *J. Am. Chem. Soc.* **2020**, *142*, 7480−7486.

(45) Li, B.; Louca, D.; Feygenson, M.; Brown, C. M.; Copley, J. R. D.; Iida, K. Local Jahn-Teller distortions and orbital ordering in $Ba_3Cu_{1+x}Sb_{2−x}O_9$ investigated by neutron scattering. *Phys. Rev. B* **2016**, *93*, 014423.

(46) Lee, K.; Kaseman, D.; Sen, S.; Hung, I.; Gan, Z.; Gerke, B.; Pöttgen, R.; Feygenson, M.; Neuefeind, J.; Lebedev, O. I.; Kovnir, K. Intricate Short-Range Ordering and Strongly Anisotropic Transport Properties of Li1−xSn2+xAs2. *J. Am. Chem. Soc.* **2015**, *137*, 3622−3630.

(47) Laurita, G.; Puggioni, D.; Hickox-Young, D.; Rondinelli, J. M.; Gaultois, M. W.; Page, K.; Lamontagne, L. K.; Seshadri, R. Uncorrelated Bi off-centering and the insulator-to-metal transition in ruthenium $A_2Ru_2O_7$ pyrochlores. *Phys. Rev. Materials* **2019**, *3*, 095003.

(48) Laurita, G.; Grajczyk, R.; Stolt, M.; Coutinho, I.; Sleight, A. W.; Subramanian, M. A. Influence of Structural Disorder on Hollandites $A_xRu_4O_8$ (A+ = K, Rb, Rb1−xNax). *Inorg. Chem.* **2016**, *55*, 3462−3467.

(49) Lamontagne, L. K.; Laurita, G.; Knight, M.; Yusuf, H.; Hu, J.; Seshadri, R.; Page, K. The Role of Structural and Compositional Heterogeneities in the Insulator-to-Metal Transition in Hole-Doped APd_3O_4 (A = Ca, Sr). *Inorg. Chem.* **2017**, *56*, 5158−5164.

(50) Karki, B.; Alfailakawi, A.; Frandsen, B. A.; Everett, M. S.; Neuefeind, J. C.; Xu, B.; Wang, H.; Fang, M.; Freelon, B. Local structure of Mott insulating iron oxychalcogenides $La_2O_2Fe_2OM_2$(M = S, Se). *Phys. Rev. B* **2021**, *104*, 064101.

(51) Dang, U.; Zaheer, W.; Zhou, W.; Kandel, A.; Orr, M.; Schwenz, R. W.; Laurita, G.; Banerjee, S.; Macaluso, R. T. Lattice Anharmonicity of Stereochemically Active Lone Pairs Controls Thermochromic Band Gap Reduction of PbVO3Cl. *Chem. Mater.* **2020**, *32*, 7404−7412.

(52) Culbertson, C. M.; Manjón-Sanz, A.; Lucero, M.; Feng, Z.; Dolgos, M. R. The local structure of $0.5Ba(Zr_{0.2}Ti_{0.8})O_3$-0.5-$(Ba_{0.7}Ca_{0.3})TiO_3$ from neutron total scattering measurements and multi-edge X-ray absorption analysis. *Mater. Res. Bull.* **2021**, *135*, 111124.

(53) Athauda, A.; Yang, J.; Lee, S.; Mizuguchi, Y.; Deguchi, K.; Takano, Y.; Miura, O.; Louca, D. In-plane charge fluctuations in bismuth-sulfide superconductors. *Phys. Rev. B* **2015**, *91*, 144112.

(54) Culbertson, C. M.; Flak, A. T.; Yatskin, M.; Cheong, P. H.-Y.; Cann, D. P.; Dolgos, M. Neutron Total Scattering Studies of Group II Titanates ($ATiO_3$, A^{2+} = Mg, Ca, Sr, Ba). *Sci. Rep.* **2020**, *10*, 3729.

(55) Zhu, H.; Yang, C.; Li, Q.; Ren, Y.; Neuefeind, J. C.; Gu, L.; Liu, H.; Fan, L.; Chen, J.; Deng, J.; Wang, N.; Hong, J.; Xing, X. Charge transfer drives anomalous phase transition in ceria. *Nat. Commun.* **2018**, *9*, 5063.

(56) Yang, L.; Koch, R. J.; Zheng, H.; Mitchell, J. F.; Yin, W.; Tucker, M. G.; Billinge, S. J. L.; Bozin, E. S. Two-orbital degeneracy lifted local precursor to a metal-insulator transition in $MgTi_2O_4$. *Phys. Rev. B* **2020**, *102*, 235128.

(57) Wang, Z.; Zhao, X.-G.; Koch, R.; Billinge, S. J. L.; Zunger, A. Understanding electronic peculiarities in tetragonal FeSe as local structural symmetry breaking. *Phys. Rev. B* **2020**, *102*, 235121.

(58) Trump, B. A.; Koohpayeh, S. M.; Livi, K. J. T.; Wen, J.-J.; Arpino, K. E.; Ramasse, Q. M.; Brydson, R.; Feygenson, M.; Takeda, H.; Takigawa, M.; Kimura, K.; Nakatsuji, S.; Broholm, C. L.; McQueen, T. M. Universal Geometric frustration in pyrochlores. *Nat. Commun.* **2018**, *9*, 2619.

(59) Shamblin, J.; Feygenson, M.; Neuefeind, J.; Tracy, C. L.; Zhang, F.; Finkeldei, S.; Bosbach, D.; Zhou, H.; Ewing, R. C.; Lang, M. Probing disorder in isometric pyrochlore and related complex oxides. *Nat. Mater.* **2016**, *15*, 507–511.

(60) Shamblin, J.; Dun, Z.; Lee, M.; Johnston, S.; Choi, E. S.; Page, K.; Qiu, Y.; Zhou, H. Structural and magnetic short-range order in fluorite Yb_2TiO_5. *Phys. Rev. B* **2017**, *96*, 174418.

(61) Shamblin, J.; Heres, M.; Zhou, H.; Sangoro, J.; Lang, M.; Neuefeind, J.; Alonso, J. A.; Johnston, S. Experimental evidence for bipolaron condensation as a mechanism for the metal-insulator transition in rare-earth nickelates. *Nat. Commun.* **2018**, *9*, 86.

(62) Mancini, A.; Barbieri, V. R.; Neuefeind, J. C.; Page, K.; Malavasi, L. Correlation between the local scale structure and the electrochemical properties in lithium orthosilicate cathode materials. *J. Mater. Chem. A* **2014**, *2*, 17867–17874.

(63) Ma, J.; Bo, S.-H.; Wu, L.; Zhu, Y.; Grey, C. P.; Khalifah, P. G. Ordered and Disordered Polymorphs of $Na(Ni_{2/3}Sb_{1/3})O_2$: Honeycomb-Ordered Cathodes for Na-Ion Batteries. *Chem. Mater.* **2015**, *27*, 2387–2399.

(64) Liu, J.; Yu, L.; Hu, E.; Guiton, B. S.; Yang, X.-Q.; Page, K. Large-Scale Synthesis and Comprehensive Structure Study of -MnO2. *Inorg. Chem.* **2018**, *57*, 6873–6882.

(65) He, A.; Bux, S. K.; Hu, Y.; Uhl, D.; Li, L.; Donadio, D.; Kauzlarich, S. M. Structural Complexity and High Thermoelectric Performance of the Zintl Phase: $Yb_{21}Mn_4Sb_{18}$. *Chem. Mater.* **2019**, *31*, 8076–8086.

(66) Dolyniuk, J.; Whitfield, P. S.; Lee, K.; Lebedev, O. I.; Kovnir, K. Controlling superstructural ordering in the clathrate-I Ba8M16P30 (M = Cu, Zn) through the formation of metal–metal bonds. *Chem. Sci.* **2017**, *8*, 3650–3659.

(67) Athauda, A.; Yang, J.; Lee, S.; Mizuguchi, Y.; Deguchi, K.; Takano, Y.; Miura, O.; Louca, D. In-plane charge fluctuations in bismuth-sulfide superconductors. *Phys. Rev. B* **2015**, *91*, 144112.

(68) Gussev, I. M.; O'Quinn, E. C.; Baldinozzi, G.; Neuefeind, J.; Ewing, R. C.; Zhang, F.; Lang, M. Local order of orthorhombic weberite-type Y_3TaO_7 as determined by neutron total scattering and density functional theory calculations. *Acta Mater.* **2020**, *196*, 704–709.

(69) Forrester, W.; Hinde, R. Crystal Structure of Barium Titanate. *Nature* **1945**, *156*, 177.

(70) Kwei, G. H.; Lawson, A. C.; Billinge, S. J. L.; Cheong, S. W. Structures of the ferroelectric phases of barium titanate. *J. Phys. Chem.* **1993**, *97*, 2368–2377.

(71) Wang, X.; Jiang, B.; Zhang, Y.; Kim, Y.-I.; Page, K. Influence of Cation Size on the Local Atomic Structure and Electronic Properties of Ta Perovskite Oxynitrides. *Inorg. Chem.* **2021**, *60*, 14190–14201.

(72) Beecher, A. N.; Semonin, O. E.; Skelton, J. M.; Frost, J. M.; Terban, M. W.; Zhai, H.; Alatas, A.; Owen, J. S.; Walsh, A.; Billinge, S. J. L. Direct Observation of Dynamic Symmetry Breaking above Room Temperature in Methylammonium Lead Iodide Perovskite. *ACS Energy Lett.* **2016**, *1*, 880–887.

(73) Kong, J.; Liu, J.; Marlton, F.; Jørgensen, M. R. V.; Pramanick, A. Local structural mechanism for phase transition and ferroelectric polarization in the mixed oxide $K_{0.5}Na_{0.5}NbO_3$. *Phys. Rev. B* **2021**, *103*, 184104.

(74) Laurita, G.; Page, K.; Suzuki, S.; Seshadri, R. Average and local structure of the Pb-free ferroelectric perovskites $(Sr,Sn)TiO_3$ and $(Ba, Ca, Sn)TiO_3$. *Phys. Rev. B* **2015**, *92*, 214109.

(75) Maughan, A. E.; Ganose, A. M.; Almaker, M. A.; Scanlon, D. O.; Neilson, J. R. Tolerance Factor and Cooperative Tilting Effects in Vacancy-Ordered Double Perovskite Halides. *Chem. Mater.* **2018**, *30*, 3909–3919.

(76) Ghosez, P.; Cockayne, E.; Waghmare, U. V.; Rabe, K. M. Lattice dynamics of $BaTiO_3$, $PbTiO_3$, and $PbZrO_3$: A comparative first-principles study. *Phys. Rev. B* **1999**, *60*, 836–843.

(77) Benedek, N. A.; Fennie, C. J. Why Are There So Few Perovskite Ferroelectrics? *J. Phys. Chem. C* **2013**, *117*, 13339–13349.

(78) Momma, K.; Izumi, F. VESTA 3 for Three-Dimensional Visualization of Crystal, Volumetric and Morphology Data. *J. Appl. Crystallogr.* **2011**, *44*, 1272–1276.

(79) Kwei, G. H.; Billinge, S. J. L.; Cheong, S.-W.; Saxton, J. G. Pair-distribution functions of ferroelectric perovskites: Direct observation of structural ground states. *Ferroelectrics* **1995**, *164*, 57–73.

(80) Ravel, B.; Stern, E. A.; Vedrinskii, R. I.; Kraizman, V. Local structure and the phase transitions of $BaTiO_3$. *Ferroelectrics* **1998**, *206*, 407–430.

(81) Comes, R.; Lambert, M.; Guinier, A. The chain structure of $BaTiO_3$ and $KNbO_3$. *Solid State Commun.* **1968**, *6*, 715–719.

(82) Redfern, S. A. T. Order-Disorder Phase Transitions. *Rev. Mineral. Geochem* **2000**, *39*, 105–133.

(83) Senn, M. S.; Keen, D. A.; Lucas, T. C. A.; Hriljac, J. A.; Goodwin, A. L. Emergence of Long-Range Order in $BaTiO_3$ from Local Symmetry-Breaking Distortions. *Phys. Rev. Lett.* **2016**, *116*, 207602.

(84) Wul, B. M.; Goldman, I. M. Dielectric Constants of Titanates of Metals of the Second Group. *Dokl. Akad. Nauk SSSR* **1945**, *45*, 154–57.

(85) von Hippel, A.; Breckenridge, R. G.; Chesley, F. G.; Tisza, L. High Dielectric Constant Ceramics. *Ind. Eng. Chem.* **1946**, *38*, 1097–1109.

(86) Gray, R. B. Transducer and Method of Making Same. U.S. Patent Appl. 2,486,560, 1946.

(87) Jeong, I.-K.; Darling, T. W.; Lee, J. K.; Proffen, T.; Heffner, R. H.; Park, J. S.; Hong, K. S.; Dmowski, W.; Egami, T. Direct Observation of the Formation of Polar Nanoregions in Pb-$(Mg_{1/3}Nb_{2/3})O_3$ Using Neutron Pair Distribution Function Analysis. *Phys. Rev. Lett.* **2005**, *94*, 147602.

(88) Fabini, D. H.; Laurita, G.; Bechtel, J. S.; Stoumpos, C. C.; Evans, H. A.; Kontos, A. G.; Raptis, Y. S.; Falaras, P.; Van der Ven, A.; Kanatzidis, M. G.; Seshadri, R. Dynamic Stereochemical Activity of the Sn^{2+} Lone Pair in Perovskite $CsSnBr_3$. *J. Am. Chem. Soc.* **2016**, *138*, 11820–11832.

(89) Laurita, G.; Fabini, D. H.; Stoumpos, C. C.; Kanatzidis, M. G.; Seshadri, R. Chemical tuning of dynamic cation off-centering in the cubic phases of hybrid tin and lead halide perovskites. *Chem. Sci.* **2017**, *8*, 5628–5635.

(90) Goldschmidt, V. Die Gesetze der Krystallochemie. *Naturwissenschaften* **1926**, *14*, 477–485.

(91) Glazer, A. M. The classification of tilted octahedra in perovskites. *Acta Crystallographica Section B* **1972**, *28*, 3384–3392.

(92) Taddei, K. M.; Xing, G.; Sun, J.; Fu, Y.; Li, Y.; Zheng, Q.; Sefat, A. S.; Singh, D. J.; de la Cruz, C. Frustrated Structural Instability in Superconducting Quasi-One-Dimensional $K_2Cr_3As_3$. *Phys. Rev. Lett.* **2018**, *121*, 187002.

(93) Qiu, X.; Proffen, T.; Mitchell, J. F.; Billinge, S. J. L. Orbital Correlations in the Pseudocubic O and Rhombohedral R Phases of $LaMnO_3$. *Phys. Rev. Lett.* **2005**, *94*, 177203.

(94) O'Quinn, E. C.; Shamblin, J.; Perlov, B.; Ewing, R. C.; Neuefeind, J.; Feygenson, M.; Gussev, I.; Lang, M. Inversion in $Mg_{1−x}Ni_xAl_2O_4$ Spinel: New Insight into Local Structure. *J. Am. Chem. Soc.* **2017**, *139*, 10395–10402.

(95) Novak, E.; Daemen, L.; Page, K.; Neuefeind, J.; Everett, M.; Egami, T.; Jalarvo, N. Temperature Dependent Local Atomic Structure and Vibrational Dynamics of Barium Hydride and Calcium Hydride. *J. Phys. Chem. C* **2021**, *125*, 24328–24339.

(96) Koch, R. J.; Konstantinova, T.; Abeykoon, M.; Wang, A.; Petrovic, C.; Zhu, Y.; Bozin, E. S.; Billinge, S. J. L. Room temperature local nematicity in FeSe superconductor. *Phys. Rev. B* **2019**, *100*, 020501.

(97) Hou, D.; Zhao, C.; Paterson, A. R.; Li, S.; Jones, J. L. Local structures of perovskite dielectrics and ferroelectrics via pair distribution function analyses. *J. Eur. Ceram. Soc.* **2018**, *38*, 971–987.

(98) Robinson, M. L.; Whitaker, E.; Jin, L.; Hayward, M. A.; Laurita, G. Evidence of Paracrystalline Cation Order in the Ruddlesden–Popper Phase $LaSr_3NiRuO_8$ through Neutron Total Scattering Techniques. *Inorg. Chem.* **2020**, *59*, 3026–3033.